Neuron, Volume *59:* Supplementary Material for

Mouse Cones Require an Arrestin for Normal Inactivation of Phototransduction

by

Sergei S. Nikonov[1], Bruce M. Brown[2], Jason A. Davis[1],

Freddi I. Zuniga[2], Alvina Bragin[1],

Edward N. Pugh, Jr.[1] & Cheryl M. Craft[2,3]

[1]F. M. Kirby Center for Molecular Ophthalmology
Department of Ophthalmology
School of Medicine
University of Pennsylvania

[2]Mary D. Allen Laboratory for Vision Research,
Doheny Eye Institute
Departments of Ophthalmology and [3]Cell & Neurobiology
Keck School of Medicine
University of Southern California

Generation and confirmation of Arr4$^{-/-}$ mice

The gene target strategy for creation of *Arr4*$^{-/-}$ mice is described in the text of the paper (text *Fig. 1*). The targeting vector was confirmed first by restriction analysis after each modification step, and then verified by dideoxy sequence analysis using primers designed to read from the *LacZ/Neo* cassette into the 3' end of the LA (LZ1) and the 5' end of the SA (N1), or from primers that anneal to the vector sequence, P6 and T7, and read into the 5' and 3' ends of the BAC subclone. Ten micrograms of the targeting vector were linearized by *Not*I and then transfected by electroporation of *129/Svev* embryonic stem (ES) cells (InGenious Targeting Laboratory Inc.). After selection in G418, 300 surviving clones were expanded for PCR analysis to identify recombinant ES clones. Oligonucleotide probes for PCR screening were as follows:

A1: 5'-CACTCAGTGCATAGAAAAGGATGG-3'

A2: 5'-TTATACAGTAAAATTTTGCAGTTG-3'

A3: 5'-GGCAATCTCAGGTACTTATAACTG-3'

AT1: 5'-ATATCTAATTTCTGAGTAAGCCTG-3'

AT2: 5'-ACAAGCATCTGTGTTGAAATTAATG-3';

N1: 5'-TGCGAGGCCAGAGGCCACTTGTGTAGC-3'.

The PCR cycling parameters: 94°C 20s; 62°C 60s; 72°C 120s; 35 cycles. ES clones (#211, 212, 233, 272, 623, 653, and 654) were identified as recombinant clones and three positive ES clones were each expanded for microinjection into *C57BL/6J* blastocysts. Chimera pups #901-907 were born and six were verified for the targeted locus by PCR genotyping.

Positive chimeras were mated with *C57BL/6* mice. Agouti F1 pups (#921-931) were genotyped. Three F1 female mice (#923, 928 and 930) were found positive for the targeted locus. These three heterozygous females were mated to *C57BL/6* males to yield the founders for the *Arr4*$^{-/-}$ colony. Three F2 litters with 22 mice were produced, with 4 male nullizygous and 5 female heterozygous KO mice, confirmed by PCR genotyping. For such genotyping,

DNA was isolated from tail clips, the amplified products were electrophoresed through agarose gels with 100bp molecular weight ladders, and an example of such confirmation is provided in ***Fig. 1S.***

Figure 1S. PCR genotype analysis of mouse visual arrestins knockouts. The genotype analyses for *Arr1* (WT allele: 280bp; KO allele: 340bp) and *Arr4* (WT allele: 750bp; KO allele: 450bp) are

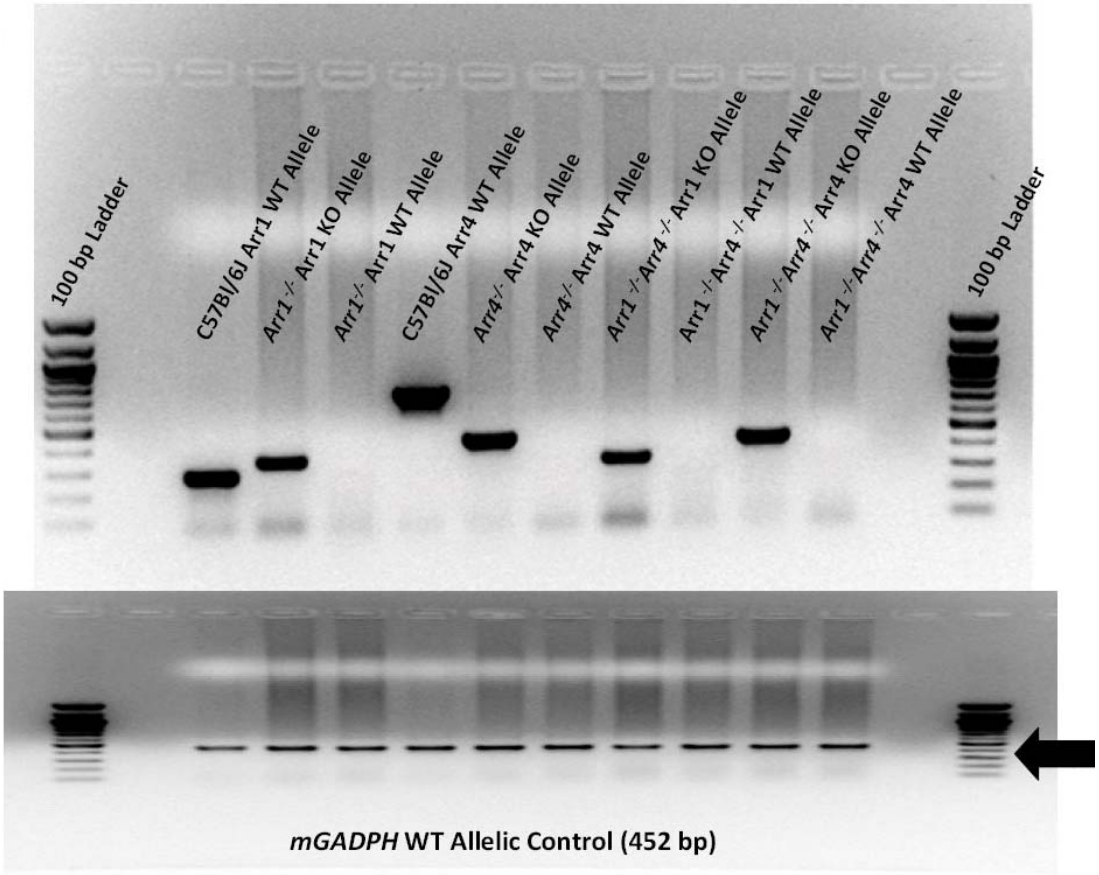

illustrated in the upper panel: lanes 1 & 4, C57Bl/6J WT control; 2 & 3 *Arr1*$^{-/-}$; 5 & 6, *Arr4*$^{-/-}$; 7, 8, 9 & 10, *Arr1*-DKO. Lower panel: *Gapdh* (Arrow: 452bp fragment) was used as a positive control to verify genomic DNA is present in each sample.

The PCR primers used for detecting the WT and knockout *Arr1* and *Arr4* alleles, and the *Gapdh* gene, and the PCR amplifying conditions are as follows.

1) ***Arr1 WT allele:*** *+Sag/Arr1 E2B and –Sag/Arr1 Tail 2; product size 280 bp,* NW_001030662.1|Mm1_11175775_37

+ *Arr1* E2B	5’-GGA CAG ACA GCA TGG CAG CCT G-3’ 22nt
- *Arr1* Tail 2	5’-GAC AAT GGG ACT GAG ATG GTG GG-3’ 23nt

2) ***Arr1 KO allele: +****Neo and –Arr1 Tail 2; product size 340 bp*

+*Neo*	5’-CCA TCT TGT TCA ATG GCC GAT CCC-3’ 24nt
- *Arr1* Tail 2	5’-GAC AAT GGG ACT GAG ATG GTG GG-3’ 23nt

3) ***Arr4 WT allele:*** *+mCAR Exon2, and -mCAR Exon5; product size 750 bp,* NT_039706.7|MmX_39746_37

+Arr4 E2	5’-GAA AGA TTC AAC TGG CCA GCA TG-3’ 23nt
-Arr4 E5	5’-GAC CCC GCG TAC TTA GAA GGT C-3’ 22nt

4) ***Arr4 KO allele: +*** *LacZA1 and -LacZS1; product size 450 bp*

+LacZA1	5’-TCG TCT GCT CAT CCA TGA CC-3’ 20nt
-LacZS1	5’-GAT TTC CAT GTT GCC ACT CG-3’ 22nt

5) ***Gapdh*** **allele:** *+mGapdh1* [570-589] and *-Gapdh2* [1021-1002], size 452 bp, NM_008084

+Gapdh1	5’-ACCACAGTCCATGCCATCAC-3’, 22nt
-Gapdh2	5’-TCCACCACCCTGTTGCTGTA-3’, 20nt

PCR conditions used for all PCR genotyping primers except Arr1 KO* primers:

2.5 μl buffer; 0.44 μl dNTP's (stock 12.5mM each); 1 μl each of the primers (10uM stock); 1.5 μl tail Genomic DNA (~1μg); 0.2 μl Taq DNA polymerase (used Lucigen EconoTaq cat # 30031-1); 18.36 μl ddH_20

PCR Program settings for Arr1 WT, Arr4 WT/KO alleles:

94^o for 2 min and 35 cycles of 60^o for 30 sec, 72^o for 50 sec, 72^o for 7 min

PCR Program settings for mGapdh WT allele:

94^o for 2 min and 30 cycles of 94^o for 30 sec, 58^o for 30 sec, 72^o for 60 sec and 72^o for 8 min

****PCR Conditions for Arr1 KO primers:***

2.5 μl buffer, 0.50 μl dNTP's (stock 12.5mM each), 1 μl of Tail2/Neo mixture (stock: 5μM each); 1.5 μl tail Genomic DNA (~1μg); 0.4 μl Taq DNA polymerase (used Lucigen EconoTaq cat # 30031-1); 19.1 μl ddH_20

****PCR Program settings for Arr1 KO allele:***

95^o for 2 min and 35 cycles of 63^o for 45 sec, 72^o for 45 sec and 72^o for 7 min

Characterization of antibodies against Arr1 and Arr4

A critical issue in the determination of the quantity of Arr4 in the retina, and in the establishment of the co-expression of Arr4 and Arr1 in cones, is the use of antibodies that discriminate between the two arrestins. Thus, we present here additional information on the two antibodies used in this investigation, LUMIj (anti-Arr4) and D9F2 (anti-Arr1).

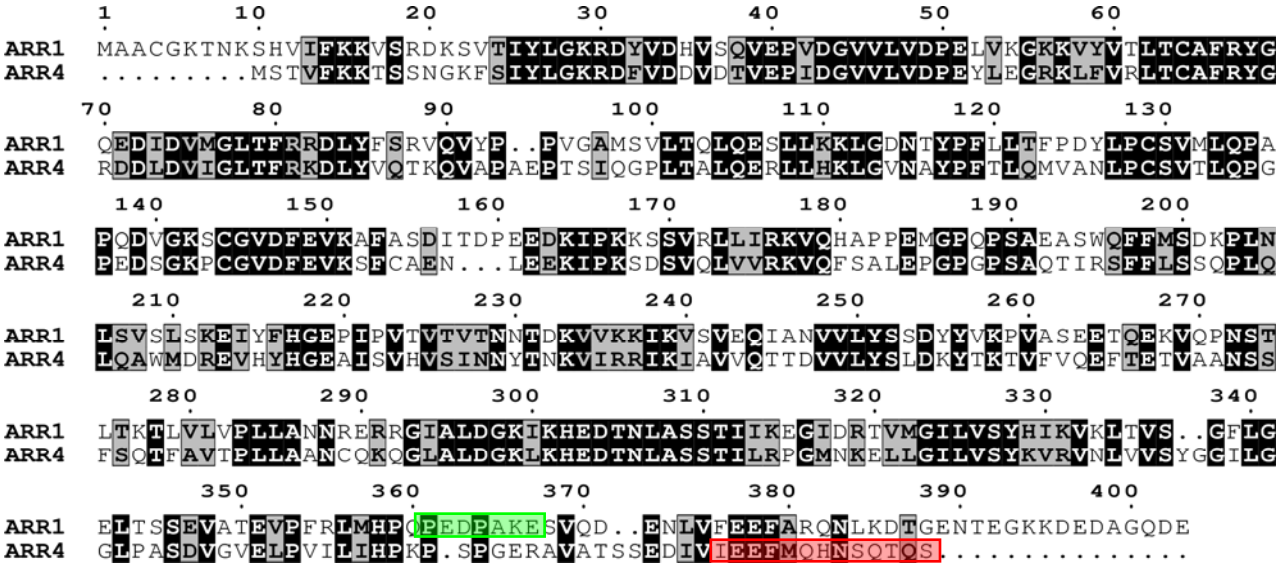

Figure 2S. Sequence alignment of mouse Arr1 and Arr4. The peptides most homologous to those used to generate the antibodies are identified by green (D9F2) and red (LUMIj) boxes, respectively. Sequence identities are highlighted in black, nonidentical, conservative regions in gray.

The monoclonal antibody D9F2 was raised against a peptide sequence of bovine S-antigen (ARR1) [AA360-368, PEDPDTAKE] (Donoso et al., 1990; Gregerson et al., 1989;Nir and Ransom, 1992), and was a generous gift of Larry A. Donoso. The rabbit polyclonal antibody LUMIj was raised against the C-terminal sequence of Arr4 (mCarr) [AA369-381, [C]EEFMQHNSQTQS](Zhu et al., 2002). Structural representations of the epitopes of Arr1 and Arr4 recognized by the two antibodies are given in ***Fig. 3S***. The structural models serve to illuminate several features of the epitopes including in particular that they are situated on the surface not directly involved in binding to rhodopsin or cone opsin (Hirsch et al., 1999)

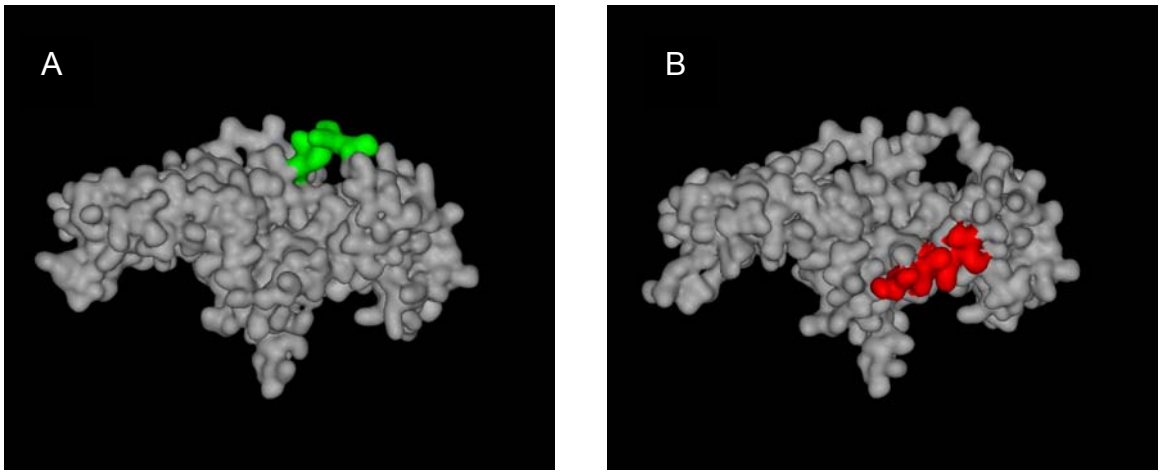

Figure 3S. **Modeled structures of *Mus musculus* Arr1 and Arr4** identifying the epitopes recognized by monoclonal antibody D9F2 (green) and polyclonal antibody LUMIj (red). Homology models of the primary sequences for the murine Arr1 (A) and Arr4 (B) were generated using high resolution structures for the corresponding proteins from *Bos taurus* ARR1 (1AYR) and *Ambylostoma tigrinum* ARR4 (1SUJ), respectively. The resulting coordinates were used to render an approximate solvent surface using Accelrys DS visualizer 1.5 (Accelrys Software Inc.). Models were generated with the Swiss-PDB server (Guex and Peitsch, 1996).

Immunoblot determination of the quantity of Arr4 per retina

Determination of the amounts of Arr4 in the mouse retina was made by quantitative Western blotting, i.e., by comparison of immunoblot signals from purified, recombinant Arr4 (rArr4) with those from retinal lysates.

Recombinant arrestins. For this study we employed two variants of recombinant Arr4: an untagged, prokaryotically expressed protein (rArr4-SG), kindly supplied by Dr. V. Gurevich, and prepared as described in Chan et al. (2007) (cf. Gurevich et al., 1999; Gurevich and Benovic, 2000), and a eukarytotically expressed, N-terminally hexahistidine- tagged recombinant Arr4 (rArr4-NTH). The rArr4-NTH was produced as follows (Davis & Pugh). Full-length cDNA for *Arr4* (genbank accession AF156979, residues 1-381) was PCR-amplified from a mouse retinal cDNA library (Pierce et al., 1999) with the 5' addition of a unique, exogenous *EcoRI* restriction site and a sequence encoding a hexahistidine tag, and with the 3' addition of a stop codon, and a unique *XbaI* restriction site. The *EcoRI-XbaI* doubly-digested PCR product was agarose gel-purified and ligated into *EcoRI-XbaI* digested, dephosphorylated pFastBac1 (Invitrogen). The plasmids were transformed into One Shot Top10 (Invitrogen) chemically competent *E. Coli* for plasmid isolation and sequence verification using automated dideoxy terminator methods. Sequence-verified plasmids were transformed into DH10Bac *E. Coli* for baculovirus production according to manufacturer's guidelines.

rArr4-NTH production and purification. Sf9 cultures were maintained in suspension culture volumes of approximately 100 ml of Sf900-II medium (Invitrogen) in 250 ml plastic flasks (Nalgene) at a density of 2.0 – 3.0x10^6 cells/ml. At a cell density of 2.0 – 2.5x10^6 cells/ml (cell viability >95%), freshly prepared high-titer baculovirus was added at multiplicity of infection empirically determined through test expression optimization of protein production. Cultures were incubated at 27°C for a further 72 – 96h. Clarified medium was applied twice to

Ni-NTA resin (Qiagen) equilibrated in 150 mM NaCl, 25 mM HEPES, pH 8.0 and allowed to flow under gravity, washed with equilibration buffer supplemented with 20 mM imidazole, and eluted with 25 mM HEPES, pH 8.0 buffer containing 300 mM NaCl, and 100 mM EDTA. The collected eluent was concentrated in Amicon Ultra 30kDA MWCO centrifuge filtration devices (Millipore) prior to loading onto a Superose 6 gel filtration column (Pharmacia) on an ÄKTApurifier UPC 10 (GE Healthcare) in 0.22 μM filtered 25 mM HEPES, pH 8.0, 150 mM NaCl. Recombinant protein eluted in the major peak and its purity was assessed by reducing SDS-PAGE: a single band was observed at the expected molecular weight (***Fig. 4S***).

Quantification of rArr4. Concentrations of rArr4-NTH stock solutions were determined spectrophotometrically on day of use, using a calculated extinction coefficient at 280 nm of 22140 $M^{-1}cm^{-1}$ (Gasteiger et al., 2005). The concentration of the untagged rArr4-SG was determined from Coomassie-stained SDS gels using (1) rArr4-NTH standards (***Fig. 4S***) and (2) BSA standards. The former determination yielded an estimate of 55 ± 4 pmol/μl (i.e., 55 μM), while the latter determination with BSA standards yielded 57 μM. Both recombinant arrestins (rArr4-SG and rArr4-NTH) were separately used in quantitative immunoblot experiments (***Table 1S***).

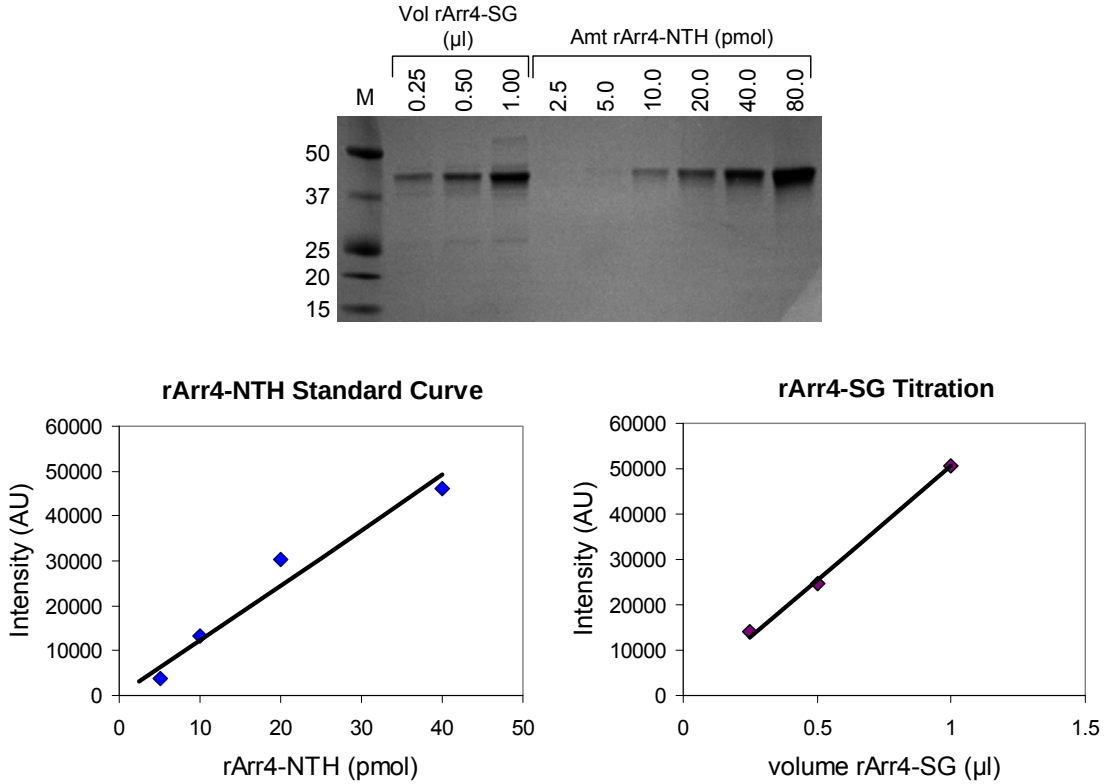

Figure 4S. **Sample Coomassie gel calibration of rArr4-SG.** Indicated volumes of untagged recombinant rArr4 (rArr4-SG) were loaded on a 4-12% gradient gel (Invitrogen) as dilutions of a supplied stock solution (lanes 2 through 4). Calibration standards consisting of the hexahistidine tagged, spectrophotometrically quantified recombinant Arr4 (rArr4-NTH) were also loaded (lanes 5 through 10) along with molecular weight standards (M – precision plus protein standards – BioRad). Band intensities on the Coomassie blue-stained gels were quantified with ImageQuant™ software and plotted over their corresponding linear ranges. The concentration of rArr4-SG in the sample was estimated to be 41.3 μM. Three such experiments yielded an estimate of 44 ± 3 μM (mean ± s.d.) Accounting for further dilution of the rArr4-SG with SDS loading buffer, the original sample is estimated to have a concentration of 55 μM.

Immunoblot quantification of Arr4 *at U. Penn.* C57Bl6 mice of 2 – 4 months of age were dark adapted for at least 24 hrs, sacrificed by CO_2 inhalation, and their eyes excised in dim red light. For each wildtype C57Bl6 determination, a corresponding dark-reared *Arr4*$^{-/-}$ mouse was similarly sacrificed and retinas excised for processing separately from the wildtype retinas. For both wildtype and *Arr4*$^{-/-}$ mice, the two retinas of each mouse were removed under infrared illumination in 150 μl of lysis buffer containing 20 mM Bis Tris propane (pH 7.5), 10 mM dodecyl β-D maltoside and 5 mM NH_2OH and a broad spectrum protease inhibitor

(Roche) and then subjected to pulsatile sonification on ice (Branson 250 Sonifier). The sonifier tip was rinsed into the tube with an additional ~50 μl of lysis buffer, and then centrifuged (Eppendorf 5415C) at 14,000 rpm at 4°C for 5 m to obtain lysate. The super-natant was then transferred on ice to a separate, pre-weighed centrifuge tube. The pellet was re-sonicated in 100 μl of lysis buffer in the original tube, the sonifier tip rinsed with 50 μl buffer, and this second tube centrifuged at 14,000 rpm at 4°C. The supernatants of the two tubes were then combined. A portion of this lysate was used to prepare a 1:10 dilution, which was subjected to bleaching difference spectroscopy to determine the rhodopsin concentration of the lysate, assuming an extinction coefficient at 498 nm of 42,000 l (mol cm)$^{-1}$ (Lyubarsky et al., 2004); rhodopsin yields ranged from 480 to 550 pmol/eye (mean 510 pmol/eye) for wildtype retinas, and 370 to 700 pmol/eye (mean 580 pmol/eye) for *Arr4*$^{-/-}$ retinas.

For immunoblotting, 5.0 to 15 μl of the lysate was combined with 8 μl of reducing dye and distilled water as appropriate to achieve a total volume of 23 μl. Calibrated quantities of rArr4 (either rArr4-NTH or rArr4-SG) were added to volumes of Arr4$^{-/-}$ lysate (proportionally, according to ratio of rhodopsin content of corresponding wildtype retinal lysate) and volumes of 5.0 to 15 μl were likewise admixed with loading dye and distilled water to a final volume of 23 μl. Standards (rArr4 + Arr4$^{-/-}$ lysate) and wildtype retinal lysate samples were boiled prior to resolution by means of 4 to 12% gradient SDS-PAGE (Invitrogen), transferred to a PVDF membrane, and analyzed using ECL detection (Supersignal West Pico Chemiluminescent Substrate, Thermo Scientific), after incubation with the anti-Arr4 polyclonal antibody LUMIj, and a secondary donkey-anti-rabbit HRP-conjugated antibody (Jackson Immunoresearch). An example of an experiment using rArr4-SG is shown in ***Fig. 5S***. Rhodopsin was measured to provide a basis for comparison among experiments, as it can be anticipated that the ratio of most retinal proteins to the quantity of rhodopsin should be invariant with dissection yield. Our

lab and others have found the adult C57Bl6 mouse retina to contain about 600 - 650 pmol rhodopsin (Lyubarsky et al., 2004).

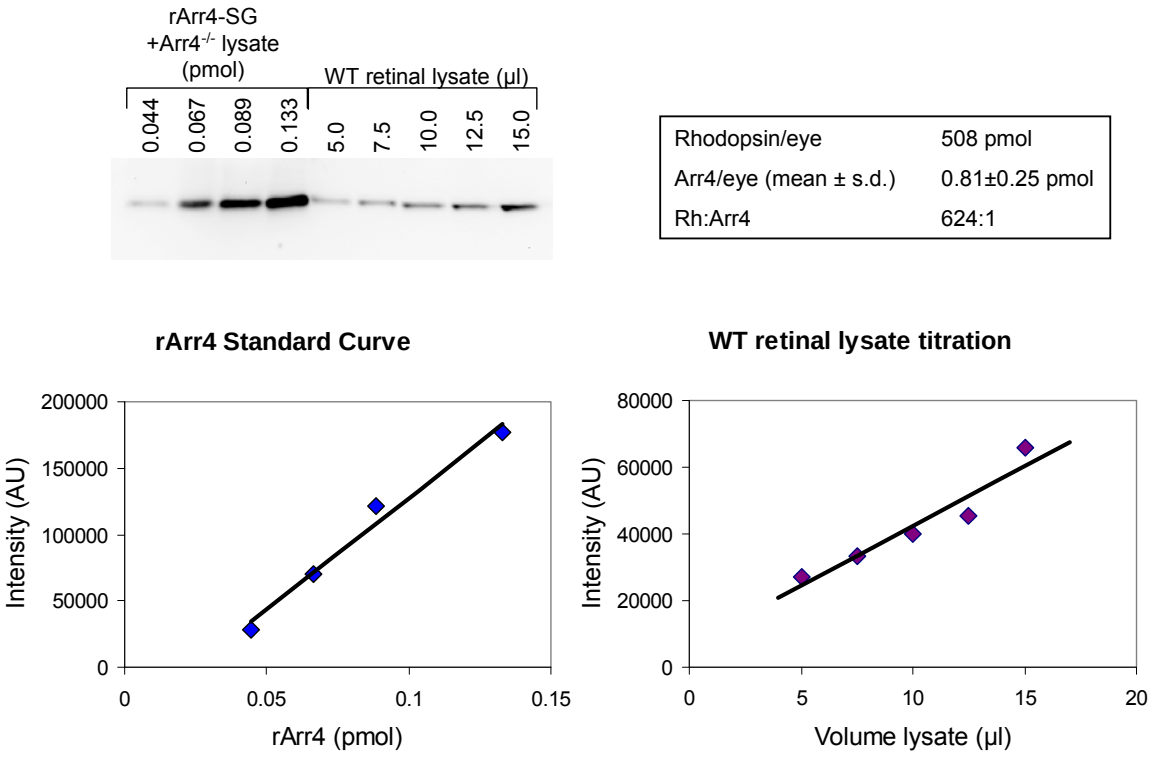

***Figure 5S*. Estimation of Arr4 in WT retina with quantitative Western blotting.** Results of a single rArr4-SG experiment. The SDS gel whose immunoblot is illustrated at upper left was loaded with rArr4-SG admixed to *Arr4*$^{-/-}$ lysate in lanes 1-4, in the indicated amounts; lanes 5-9 were loaded with WT retinal lysate of the specified volumes. The blot signal intensities, extracted with ImageQuant™ software, are shown in the two plots below the Western blot. Since the blot signals of the WT lysates lie within the linear range of the rArr4-SG blot intensities, the estimates of Arr4 in the WT lysate could be extracted by the position on which they fall on the regression line through the rArr4-data. In this experiment the total extracted rhodopsin was determined to be 508 pmol/eye. *Arr4*$^{-/-}$ lysate was mixed with rArr4-SG in a master sample so that the ratio of Rh:rArr4-SG was approximately 340:1, obtained from a prior approximate estimation. The Rh:Arr4 ratio in the WT retina was thus estimated to be 624:1, or ~ 1 pmol/eye in an eye with 600 pmol Rh.

Immunoblot quantification of Arr4 at U.S.C and UC Davis. A protocol similar to that used at Penn for preparing retinal lysates and performing quantitative immunoblotting with rArr4-SG was employed at U.S.C. (Brown & Craft) and UC Davis (Burns & Pugh). In the former case, however, rhodopsin was not measured and the results are thus reported in pmol Arr4/eye

(***Table 1S***); rhodopsin measurements and quantitation in the latter case (UC Davis) were performed according to the protocols described in (Krispel et al., 2006). Detection of signals on western blots employed ECL substrate at U.S.C., while the work at UC Davis employed infrared fluorescent detection using the LiCor™ blotting system.

The results of all experimental efforts to quantify Arr4 in this study are summarized in ***Table 1S***, along with results from other investigations. Results in this study comprise both chemiluminescent (Brown, Yetemian & Craft; Davis & Pugh) and infrared fluorescent (Burns & Pugh) means of signal detection on immunoblots, and include both prokaryotic, untagged recombinant protein, as well as eukaryotically expressed, N-terminally hexahistidine tagged protein. As can be seen, independent investigations at separate institutions involving various combinations of these methods of detection and recombinant proteins yield similar estimates of the total quantity of Arr4 in the WT mouse retina, but differ from the estimate previously published by Chan *et al*. (2007) by about 100-fold. No incontrovertible explanation can be provided for this discrepancy, however the following, individually or in combination, offer some possibilities. First, the retinal yields in the work of Chan *et al.* may have been lower than those of the present study where, in the absence of rhodopsin quantification, we assumed the yield be 2/3 (i.e., 400 pmol rhodopsin); however, Chan et al. report only 80 pmol Arr1/retina, while if the Rh:Arr1 ratio is 1:1.3 (Strissel *et al*., 2006), a 400 pmol yield of rhodopsin predicts that 308 pmol Arr1 would be extracted. Second, since Chan *et al.* (2007) did not have access to *Arr4*$^{-/-}$ mice, the masking effect of retinal lysates could not be controlled; in the present study, this effect was observed to be as large as 20-fold (data not shown). Finally, the difference in methods employed to quantify the concentration of the rArr4 protein solution should be noted. In the present study, the purity of the rArr4-NTH permitted its quantification using UV absorption spectroscopy with a calculated extinction coefficient. The presence of other proteins in the provided rArr4-SG sample precluded use of this method.

Table 1S. Estimates of the quantities of Arr1 and Arr4 in the mouse retina

Reference	n	Arr1:Rh	Arr1/retina (pmol)	Arr1/rod (#)	Protein & Quantification
Strissel *et al.* (2006)	2	**1:1.3**	460	$4.3x10^7$	N-term-hexaHis tagged Arr1, UV abs
Hanson *et al.* (2007)	7	**1:1.2**	500	$4.7x10^7$	rArr1 (as published)
Chan *et al.* (2007)	1	1:5	**120**	$1.1x10^7$	rArr1 (as published)

Reference	n	Arr4:Rh	Arr4/retina (fmol)	Arr4/cone (#)	Protein & Quantification
Chan *et al.* (2007)	1	1:67000	**9**	$2.7x10^4$	rArr4-SG (as published)
Brown *et al*. (this study)	1	1:630	**950**	$2.9x10^6$	rArr4-SG, Coomassie gel
Burns & Pugh (this study)	2	**1:560**	1070	$3.2x10^6$	rArr4-SG, Coomassie gel
Davis & Pugh (this study)	5	**1:740**	810	$2.5x10^6$	rArr4-SG, Coomassie gel
Davis & Pugh (this study)	5	**1:430**	1380	$4.2x10^6$	rArr4-NTH, UV abs

Table notes. Results are presented for measured quantity of Arr1 or Arr4 reported in the literature, and determined in the present study, along with the number of measurements comprising each value (n). Columns 3 and 4 specify the quantity of Arr1 or Arr4 in two interconvertible ways: relative to rhodopsin (col 3), or per retina (col 4); the measurement reported by the authors is shown in bold print, while the derived quantity is in plain print. To make the interconversions, it is assumed that the C57BL/6 mouse retina has 600 pmol rhodopsin (Lyubarsky et al., 2004), but, where rhodopsin yield was not quantified, that a typical retinal dissection would yield ~ 400 pmol. To calculate the values in column 5, the number of rods in the C57BL/6 retina was taken to be 6.4×10^6 and cones 200,000 (Jeon *et al.*, 1998). Also indicated for each study is recombinant protein used in the quantitative western blotting, and the method by which its concentration was quantified (where available).

Instead, intensities on Coomassie-stained gels using standards of either BSA (n=1, data not shown) or rArr4-NTH (n=6, ***Fig. 4S***) were used to estimate the concentration of rArr4-SG and yielded values in very close agreement. Thus, the reported ratio of Arr4 relative to rhodopsin for this study is taken as the weighted average of the determinations (excluding that by Chan *et al.*), namely 1.1 $\pm$ 0.2 (mean $\pm$ 2 s.e.m.) pmol Arr4 in a retina containing 600 pmol rhodopsin, yielding a ratio of Rh:Arr4 ~ 550:1.

In ***Table 1S*** published data are also summarized in which the quantity of Arr1 in the retina was estimated with quantitative immunoblotting. For subsequent analyses in this study, the value of Strissel *et al.* (2006) (Rh:Arr1 = 1.3:1) was adopted in the quantification of Arr1 in cone photoreceptor cells with immunofluorescence (see below "*Estimation of the quantity of Arr1 in cones with two-color immunofluorescence"*). It bears mention that we employed essentially the strategy used by Strissel *et al.* (2006), including the use of an N-terminal, hexahistidine tagged recombinant standard quantified by absorbance at 280 nm (with the exception that Arr4-NTH was expressed in a eukaryotic, not bacterial, cell line). Moreover, we close by noting that Strissel *et al*. did not include the absorbance of the TEV linkage peptide sequence in their spectrophotometric quantification of their rArr1 (Sokolov & Arshavsky, personal communication), employing an absorbance ε_{280} = 22810 l (mol cm)$^{-1}$, when the calculated absorbance based on the sequence predicted from the expression vector is ε_{280} = 31,080 l (mol cm)$^{-1}$. This miscalculation produces an overestimate of the quantity of rArr1 by 36% (= 100 x (1 – 31080/22810), and thus requires the Arr1: Rh ratio to be corrected from 0.78:1 to 0.6:1. In the end, however, we adopted the uncorrected value of Strissel *et al.* (2006), as it lies approximately midway between the corrected estimate and the later estimate by (Hanson et al., 2007)..

Specificity of immunofluorescence measured with LUMIj and D9F2 antibodies

The specificity of the antibodies LUMIj and D9F2 for Arr4 and Arr1 respectively was established under the conditions of histochemical imaging (as illustrated in *Fig. 2* of the text). In brief, the identical protocol of immunostaining and confocal imaging (Methods) was applied to cryosections of retinas of WT, *Arr4*$^{-/-}$, *Arr1*$^{-/-}$ and *Arr*-DKO mice, and the results compared, as now described. (In what follows, for simplicity we will not refer to the secondary antibodies explicitly, but rather simply specify the fluorochromes to which they are conjugated, thus "LUMIj-Alexa555" refers to the rabbit pAb LUMIj bound to anti-rabbit IgG conjugated to Alexa555, and "D9F2-Alexa488 refers to the mouse mAb D9F2 bound to anti-mouse IgG conjugated to Alexa488.)

Non-specific fluorescence. To determine whether contributions to fluorescence from non-specific binding of the primary antibodies and/or secondaries, or from autofluorescence, might interfere with immunofluorescence quantitation, we analyzed and compared histograms of the fluorescence distributions of the Alexa555 ("red") and Alexa488 ("green") channels from the confocal images of the cryosections of WT and *Arr*-DKO mice (***Fig. 6S***). These histograms confirm quantitatively what can be seen qualitatively in the corresponding images (cf. *Fig. 2* of the text): in all retinal layers non-specific fluorescence (i.e., that arising from combined autofluorescence and fluorescence from non-specific retention of the antibodies) was well less than 10% of that recorded when Arr1 and Arr4 are present. Thus, comparison of the two histograms in each panel shows the non-specific fluorescence in either the D9F2-Alexa488 or the LUMIj-Alexa555 channel to be confined to the lowermost histogram bins. Indeed, in most portions of the images, the non-specific fluorescence distribution of the *Arr*-DKO cryosections overlapped those of the WT by less than 5%.

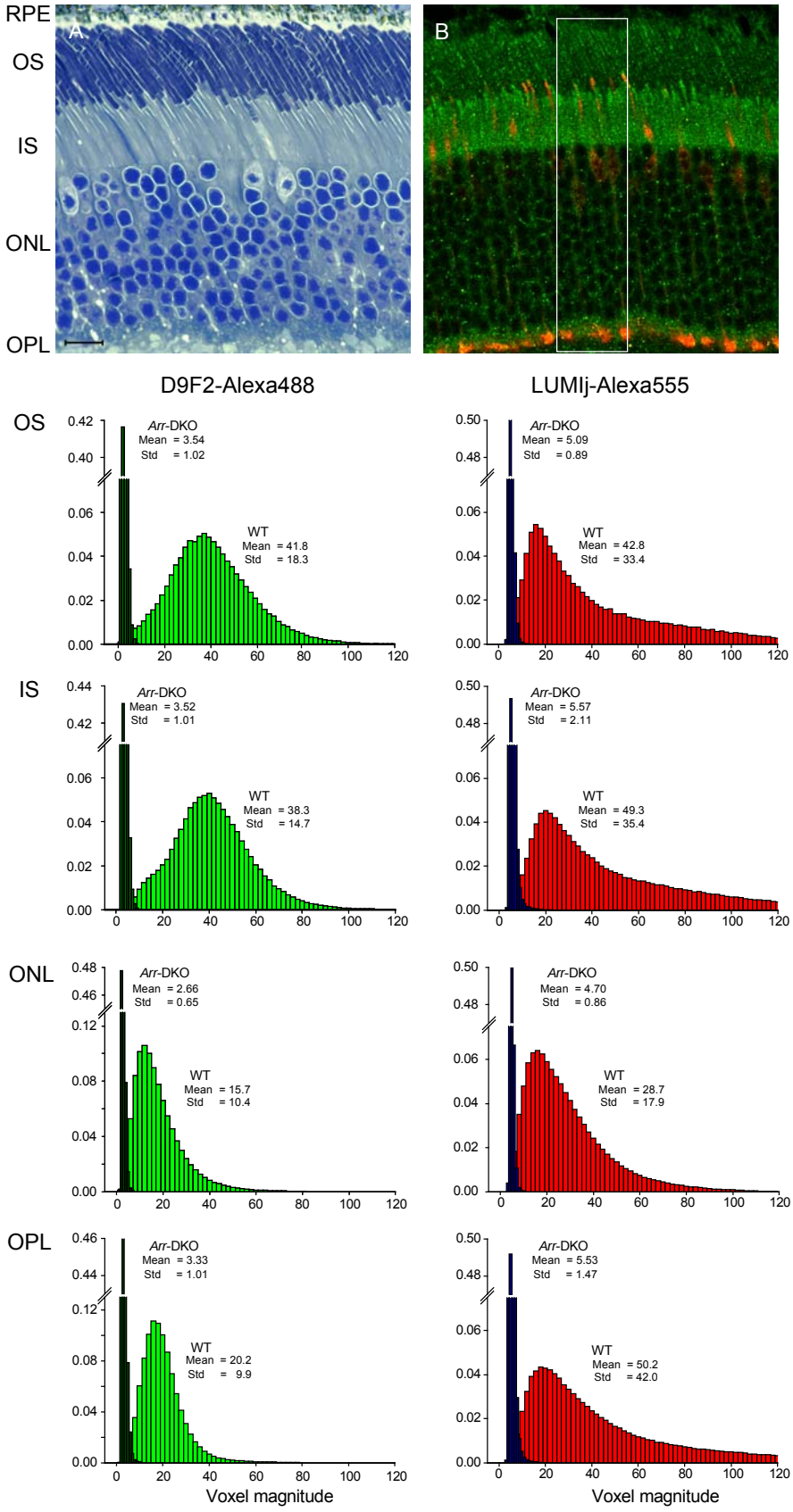
RPE
OS
IS
ONL
OPL
A
B
D9F2-Alexa488
LUMIj-Alexa555
OS
IS
ONL
OPL
Arr-DKO
Mean = 3.54
Std = 1.02
WT
Mean = 41.8
Std = 18.3
Arr-DKO
Mean = 5.09
Std = 0.89
WT
Mean = 42.8
Std = 33.4
Arr-DKO
Mean = 3.52
Std = 1.01
WT
Mean = 38.3
Std = 14.7
Arr-DKO
Mean = 5.57
Std = 2.11
WT
Mean = 49.3
Std = 35.4
Arr-DKO
Mean = 2.66
Std = 0.65
WT
Mean = 15.7
Std = 10.4
Arr-DKO
Mean = 4.70
Std = 0.86
WT
Mean = 28.7
Std = 17.9
Arr-DKO
Mean = 3.33
Std = 1.01
WT
Mean = 20.2
Std = 9.9
Arr-DKO
Mean = 5.53
Std = 1.47
WT
Mean = 50.2
Std = 42.0
Voxel magnitude
Voxel magnitude

Figure 6S. **Confirmation that neither autofluorescence nor non-specific binding affects the signals recorded with D9F2-Alexa555 and LUMIj-Alexa555.** The upper left panel shows a plastic section of a retina for identification of the layers, while that at right repeats text *Fig. 2* in which a cryosection of WT retina has been immunostained with both D9F2-Alexa488 and LUMIj-Alexa555. The remaining panels present pairs of histograms of the fluorescence of 8 cones from the z-stack of the WT retinal section illustrated (above right) or from the z-stack of the *Arr*-DKO section of text *Fig. 2*; the cones were "cut out" of the stack with the "two-color cookie cutting method" described in Methods and in this Supplement, whereas the *Arr*-DKO data were collected from a 3D-slab spanning ~ 100 μm x 15 μm in the *x*- and *y*- dimensions (white frame in image at upper left) and 1.8 μm thickness (spanning 7 z-stack sections) . The panels in the left column are histograms of fluorescence collected in the Alexa488 ("green") channel of the LSM-510 confocal microscope, while the panels at right give histograms for LUMIj-Alexa555 ("red" channel); the mean and standard deviation of each histogram are given next to it. For each pair of histograms it can be seen that the histograms of the *Arr*-DKO cryosection (darker colors) has minimal overlap with that of the WT cones (bright green, D9F2-Alexa488, or bright red, LUMIj-Alexa555). Each histogram comprises the intensity of several hundred thousand voxels; the ordinates are given as fractions of the total count (i.e., the data are presented as density functions).

Specificity of the LUMIj and D9F2 antibodies for Arr1 *and* Arr4*, respectively*. The specificity of the LUMIj and D9F2 antibodies for their target antigens Arr4 and Arr1 was confirmed by comparison of the fluorescence distributions of LUMIj-Alexa555 and D9F2-Alexa488 in the different sublamina of the photoreceptor layer of mice of the four genotypes, WT, *Arr4*$^{-/-}$, *Arr1*$^{-/-}$ and *Arr*-DKO (***Fig. 7S***). The histochemical method is identical to that used for the images presented in *Figs. 2 & 3* of the text, and the histogram analysis employed the same as that used in ***Fig. 6S*** above. To simplify the presentation, in ***Fig. 7S*** we provide only the mean and standard deviation of the distributions, rather than the entire distributions (histograms). The critical feature of this analysis is obtained from comparison of *Arr1*$^{-/-}$ and *Arr4*$^{-/-}$ sections: in each case and for each fluorochrome, the fluorescence that would be ascribed to the absent species of arrestin is negligible, i.e., is equivalent to the non-specific fluorescence of the *Arr*-DKO (dashed lines), while the fluorescence ascribable to the species of arrestin present is reliably detected and comparable to that of the WT. In sum, under these conditions each antibody reports only the presence of its specific antigen target.

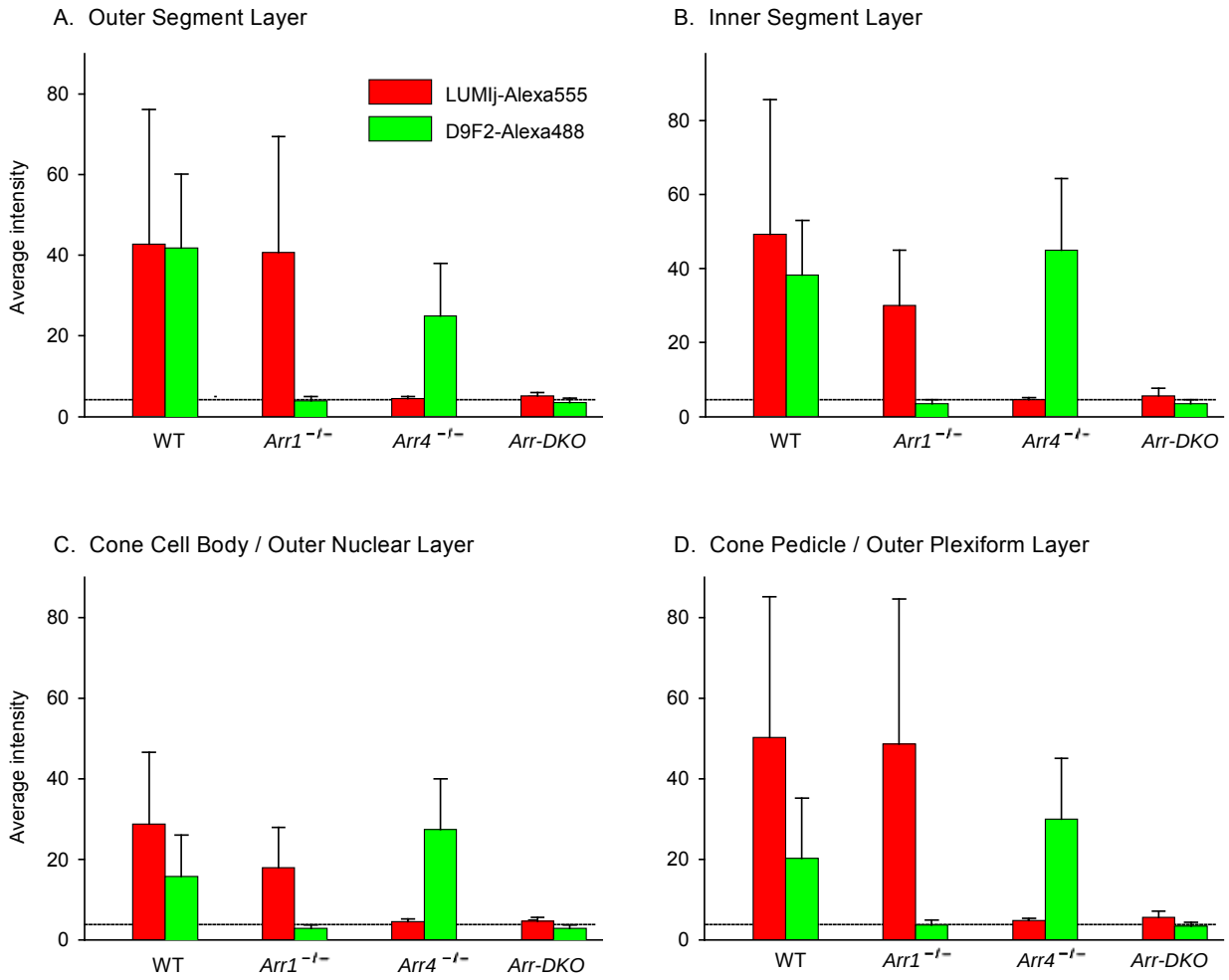

Figure 7S*. Confirmation of histochemical specificity of LUMIj and D9F2 antibodies for Arr4 and Arr1 respectively**. Each panel shows the average fluorescence intensity (mean + s.d.; in units of the 8-bit or 0 – 255 display) of voxels of cryosections exposed to the two antibodies and imaged with the confocal microscope under identical conditions. For sections of WT and *Arr1*$^{-/-}$ mice, the voxels were from a population of 8 cones that were "cookie cut" from the 3D z-stacks of *Fig.* 3 of the text, with the LUMIj antibody allowing visualization of the cone envelope. For sections of *Arr4*$^{-/-}$ and *Arr*-DKO mice, the voxels analyzed were from 3 μm thick confocal "slabs" (as in panel B of *Fig.* 3 of the text, and in ***Fig. 6S panel B, and the layers were identified by either the D9F2 fluorescence distribution or by structure markers). The dashed line in each panel indicates the level of non-specific fluorescence, as established in ***Fig. 6S***. We emphasize that there is no cross-talk between Alexa488 and Alexa555 fluorescence, due both to the different excitation wavelengths employed, 488 nm vs. 543 nm, respectively, and to the fluorescence collection bands, 515 nm to 530 nm and 560 to 600, respectively: thus, Alexa488 has negligible excitation at 543 and Alexa555 has minimal (~15% of max) excitation at 488, while Alexa488 has nil emission above 550 nm and Alexa555 nil emission below 550 nm.

Estimation of the quantity of Arr1 in cones with two-color immunofluorescence

As presented in the context of *Fig. 3* of the text, the confirmed specificity of the LUMIj and D9F2 antibodies made it possible to estimate the quantity and distribution of Arr1 in WT cones. This was achieved with an approach embodying the following three steps: (1) extraction of the immunofluorescence distribution in cones of D9F2-Alexa488 by "two-color cookie cutting" of high resolution confocal images, in which the voxels of the cone, determined by immunofluorescence of Arr4-LUMIj-Alexa555 (see text *Fig. 3B, C*), are extracted; (2) quantitation of the fluorescence per molecule of Arr1 by analysis of the fluorescence intensity of "slabs" of inner segments, where Arr1 is expressed at a high level and nearly uniformly in the dark adapted retina; (3) conversion of the distribution of D9F2-Alexa488 immuno-fluorescence in cones into local concentrations, summing over the compartments (as in Peet et al., 2004). These steps will now be explained in greater detail, followed by some caveats.

Two-color cookie cutting. The first step in estimation of the quantity of Arr1 in WT mouse cones was determination of the D9F2-Alexa488 immunofluorescence distribution inside the cone envelope, as extracted with high resolution confocal imaging. The results of application of this method are illustrated in *Fig. 3* of the text (see also Methods). For the Zeiss LSM-510 confocal that was used with a 63X oil immersion objective, the 3D point-spread function (volume probed by the focused laser beam) is approximately a Gaussian ellipsoid having standard deviations in *x*- and *y*- (the image plane) of about 0.15 μm and in *z*- of about 0.3 μm (Pawley, 2007). Because Arr4-LUMIj-Alexa555 fluorescence is present in virtually all compartments of the cone cytoplasm, the envelope of the cone is well determined to within ~ 0.2 μm, and so, having isolated in 3D the voxels producing Alexa555 fluorescence, these same voxels can be interrogated for their Alexa488 fluorescence, and thus for the presence of D9F2 antigenicity. There is inevitable volumetric distortion, however, of small diameter objects such as the OS (1.2 μm) diameter and the cone axon.

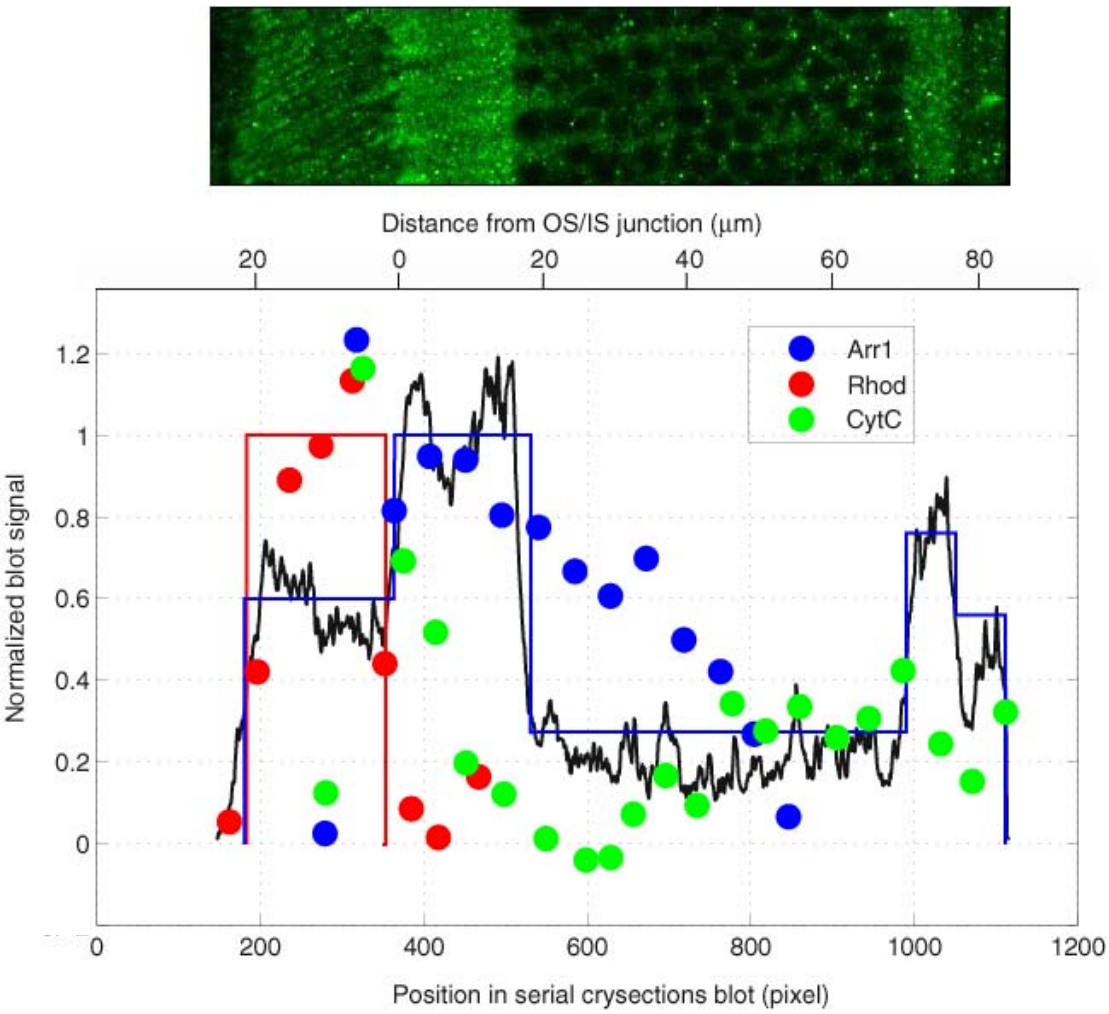

Figure 8S*. Comparison of the immunofluorescence distribution of the Arr1 mAB D9F2-Alexa488 with the retinal serial cryosection data of Strissel *et al. (2004, Fig.1, panel B, "0% bleaching"). The symbols plot the blot densities of the serial cryosections (taken at 5 μm increments from the rod tips), reacted with antibodies to Arr1 (•), Rhodopsin (•) and Cytochrome C (•) of each section. The noisy black trace plots the immunofluorescence of D9F2-Alexa488 in the confocal image of a "slab" of a retinal cryosection (image at top, from *Fig. 2B* of the text, portion of image outlined in white, upper abscissa). The four sets of data have been scaled to approximately unity amplitude at the region corresponding to the inner segments of the rods. The uninterrupted red trace is an idealized distribution of rhodopsin and the blue trace an idealized distribution of Arr1 consistent with the black trace. There are three notable areas of discrepancy between the serial crcryosection data and the trace from the histochemical "slab" analysis: first, Strissel *et al*. report that Arr1 in the OS is no more than 7% of the total in the dark adapted rod, while our grand average estimate is 12.5% (Table 1); second, the Arr1 quantities observed by Strissel *et al*. decline gradually in the ONL, whereas our immunofluorescence data undergo a stepwise drop from the IS layer; third, Strissel *et al*. report little Arr1 near the rod synaptic region, whereas the immunofluorescence shows a very clear jump in this region. Overall, these discrepancies do not seriously alter the conclusion critical for our quantitation, viz. that roughly 30% of Arr1 is in the inner segment layer of a dark adapted mouse retina.

Quantitation of the Alexa488 fluorescence per unit concentration of Arr1. D9F2-Alexa488 emission inside the "cookie cut" cone boundary can be used to estimate the absolute quantity of Arr1, providing a quantitative scale can be developed relating D9F2-Alexa488 fluorescence to Arr1 concentration (keeping in mind that the confocal imaging probes the local concentration of fluorochrome in the sample voxel). We (and others) have previously shown such quantitation to be possible with fluorochromes such as EGFP, and used the method to quantify the distribution and movement of ARR1-EGFP fusion protein in *Xenopus* rods (e.g., Peet et al., 2004), and many papers in which the "relative" distribution of Arr1 in the retina has been quantified on the basis on immunofluorescence (e.g., Hanson et al., 2007;Kassai et al., 2005;Nair et al., 2005). In the approach used here, the critical assumption is that the concentration of Arr1 in the dark adapted mouse retinal inner segment layer can be derived, as follows. We assume the ratio Arr1:Rh in the mouse retina is 0.78: 1 (Strissel *et al*., 2006), and that the retina of the normal C57BL/6 mouse (age 6 – 8 weeks) contains about 600 pmol rhodopsin (Lyubarsky *et al*., 2006), implying a total quantity of Arr1 of 470 pmol per eye. To estimate the fraction of Arr1 in the inner segment layer, we analyzed the radial distribution of Arr1-D9F2-Alexa488 fluorescence in thin confocal "slabs" (see text *Fig. 3B; 3D*) and compared this distribution with the serial cryosection data of Strissel *et al*. (***Fig. 8S***). The comparison, though imperfect, is broadly consistent with the conclusion that about 30% of the total Arr1 in the dark adapted retina is in the IS layer, and so we conclude that the concentration of Arr1 in the dark adapted IS layer is 460 μM. This latter concentration is arrived at from the dimensions of the IS layer (about 18 μm; ***Fig. 6S, A, B***): thus, in an eye where the retina is a hemispherical surface of about 17 mm^2 (Lyubarsky et al., 2006), the IS layer has a volume of 17 x 10^6 μm^2 x 18 μm = 3.06 x 10^8 μm^3 = 3.06 x 10^{-7} liters, and so the Arr1 concentration in the IS layer in the dark adapted retina is (0.3 x 470 x 10^{-12} mol) / (3.06 x 10^{-7} liters) = 460 μM.

Quantification of Arr1 *in cones*. The third step in estimating the quantity of Arr1 in cones is based on the relative fluorescence intensity of adjacent rods and cones immunoreacted with the Arr1-specific antibody D9F2. Thus, in a given cryosection we determined the average fluorescence intensity of D9F2-Alexa488 in the inner segment layer in a "slab", and assumed that this corresponds to that from 460 μM Arr1, thus setting an absolute scale factor for converting D9F2-Alexa488 immunofluorescence per voxel into molecules of Arr1 per voxel. Using the two color-cookie cutting method, the fluorescence of D9F2-Alexa488 in 21 cones of the same three z-stacks used for the Arr4 analysis was determined, and the derived scale factor for each stack used to determine the quantity of Arr1 in each cone (Table 1 of the text).

Caveats. Given the specificity that we established of the LUMIj and D9F2 antibodies for Arr4 and Arr1 respectively (***Figs. 6S, 7S***), the principal assumption of the method used to determine the Arr1 expression level in cones is that the concentration of Arr1 in the dark adapted inner segment layer is well determined (as described above). Another assumption is that the access of D9F2 antibody is equal in adjacent rods and cones in the cryosection, in other words, that there is no differential epitope masking. This latter assumption can be challenged, but as we report here (***Fig. 8S***), the distribution of Arr1 immunofluorescence in cryosections corresponds reasonably well with that determined from serial crysection data and the immunoblotting method of (Strissel *et al*., 2006), and complements it, in revealing details of the Arr1 distribution that are beyond the resolution of the cryosection method, and points to some of its limitations.

Control Electrophysiology Experiments

An important issue in electrophysiological experimentation is the stability of the preparation over the time course of experimentation. This issue is of particular importance in recordings from mouse cones, plagued early attempts to use suction pipettes to record currents from cone outer segments, and led to the development of a recording method in which the inner segment and/or perinuclear region is drawn into the suction pipette (Nikonov

et al., 2005;Nikonov *et al*., 2006), which yielded stable, long-term recordings. Nonetheless, as we introduce here for the first time recordings from cones from which critical cone-specific proteins, Arr4 and Arr1, have been deleted, we felt it important to document the stability of the recordings (***Figure 9S***).

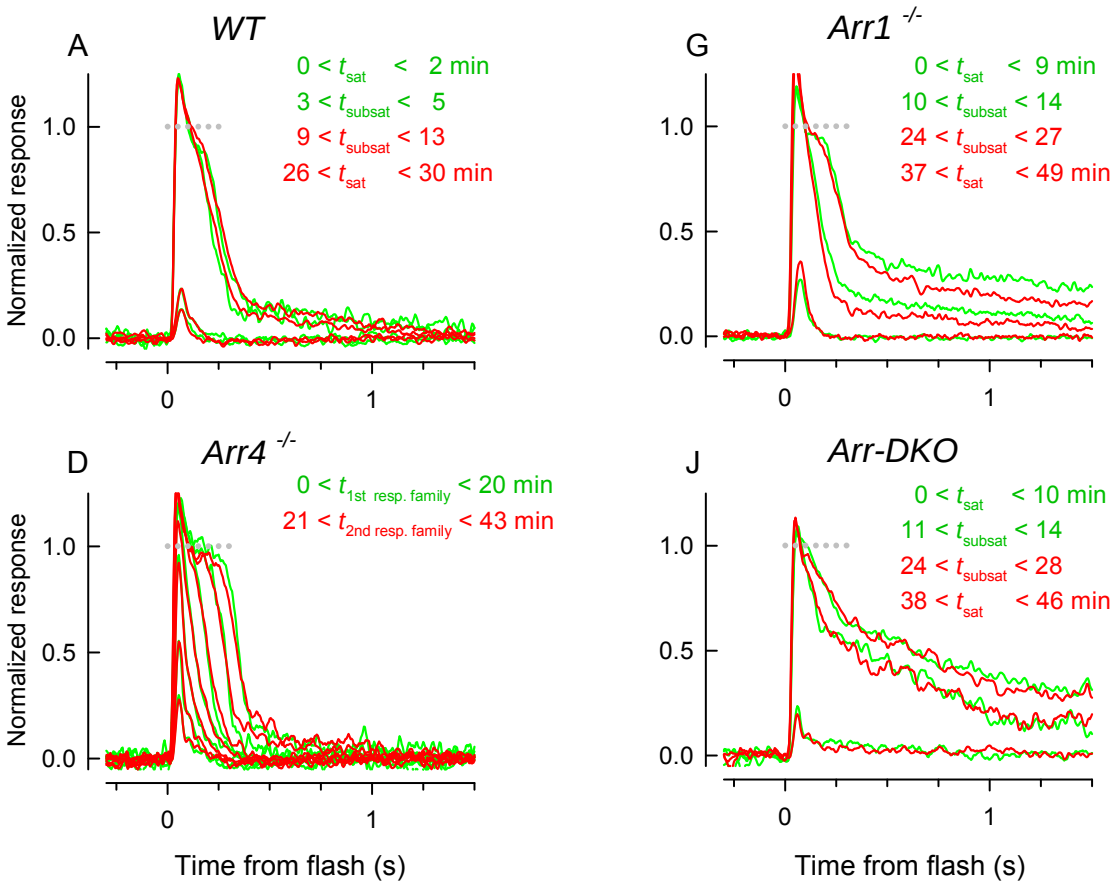

Figure 9S. **Response properties of WT and cones with Arr4 and Arr1 deleted were highly stable over the recording session**. Responses of the same cones whose data are presented in *Fig*. 4 of the main text are illustrated. Test saturating responses were recorded at the beginning and at the end of the recording session, and test subsaturating responses were recorded correspondingly after the first set and before the final set of saturating responses. Here green traces show averaged responses recorded at the start of the experiment and red traces show averaged responses recorded at the end of the recording session. The time intervals during which the responses were recorded (in min from the start of the experiment) for each set of traces are given on the figure. For the *Arr4*$^{-/-}$ cone (from panel D of text *Fig*.4) a complete response family was recorded at the beginning and end. For the illustrated traces, 15-50 individual responses to the subsaturating flashes were averaged, while 7-20 responses were averaged for responses to the saturating flashes. As can be seen, the responses to both dim and bright flashes were stable for periods of 30 to 49 min, regardless of genotype. (The panels are labeled with the same letters used in *Fig*. 4 of the main text.)

Analysis of the light-sensitive current

Traditionally, "photocurrents" (i.e., the suppression of the circulating current) of mouse rods have been recorded by drawing the outer segment into the suction pipette. As mentioned above, this method cannot be readily used for recording mouse cone photocurrents, and we developed a method of recording from the "inner segment" (Nikonov *et al*., 2005;Nikonov *et al*., 2006). A drawback of the latter method is that the plasma membrane of the inner segment and perinuclear region of the photoreceptor contains voltage-activated channels whose currents to some degree distort the responses that would be observed in their absence. To make it clearer why we normalized the light-response families as we have (*Fig*. 4 of the text) to extract the amplification, we present an experiment that illustrates how we identified the light-sensitive component of the current (***Fig. 10S***).

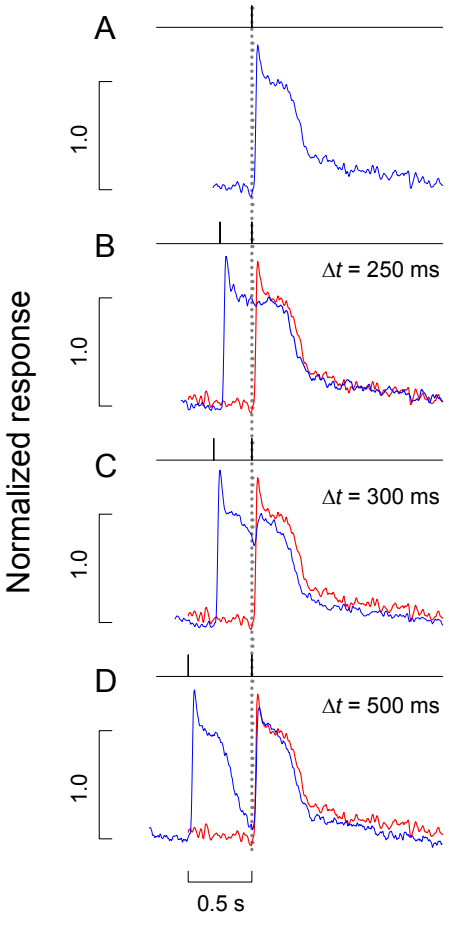

Figure 10S. **Paired flash experiment illustrating the identification of light-sensitive current.** Responses of a cone to paired flashes of light. The blue trace in each panel is a response to one (A) or a pair (B-D) of identical flashes delivered with the indicated time separation (Δt); the red trace is a copy of the response to the single flash shown in panel A, but located at the point of the delivery of the second flash. Note that in panel B, when the second flash is delivered at Δt = 250 ms during the plateau phase, there is no "nose" on the response; the reappearance of the nose corresponds with the recovery of the response below the plateau (panels C, D). Thus, the plateau defines the zero level of the light-sensitive current, and the nose represents a current likely activated by hyperpolarization caused by the flash. Each trace is the average of at least 15 responses.

Thus, the "nose" above the plateau is not light-sensitive current, but rather current that flows through the membrane in the suction pipette presumably in response to the light-evoked hyperpolarization. Hence, it would be incorrect to include this component in the normalization required for the amplification analysis. The nature of the "nose" current has been investigated in a number of previous publications, and the generally accepted explanation is a hyperpolarization-activated I_h inward current, followed by a net outward current resulting from initial inactivation of I_{Kx} currents, diminishment of I_h as the cone depolarizes toward $E_{h,rev} \approx$ -30 mV, and reactivation of I_{Kx}. (See review by Barnes, 1994).

Phylogenetic analysis of "Cone Arrestin"

The phylogenetic status of "rod" and "cone" arrestins has been the subject of a number of inquiries and discussed previously (Craft and Whitmore, 1995;Gurevich and Gurevich, 2006). With the current understanding that cone-like photoreceptor cells anteceded rods in the evolution of the retina (Reichenbach and Robinson, 1995; Lamb *et al*., 2007), and the curious finding that both Arr1 and Arr4 are expressed in functionally relevant concentrations in mouse cones, we revisited the phylogenetic issue (***Fig. 11S***). What is apparent in this unrooted tree is that the ARR4 and ARR1 subfamilies of the lower vertebrate species appear to have diverged to about the same degree from the single arrestin (Ci-Arr), of the tunicate *Ciona intestinalis*. Tunicates are chordates that emerged in the pre-Cambrian period prior to two genome-wide duplication events that occurred between their emergence and that of bony fishes (Delsuc *et al*., 2006; Sidow, 1996). Nonetheless, it seems likely that the precursor of ARR4 emerged somewhat earlier than ARR1. This follows, since the photoreceptors of extant lampreys – jawless vertebrates that emerged in the Cambrian – are cone-like at the structural and molecular level (reviewed in Lamb *et al*., 2007). Another remnant of the prior emergence of ARR4 may be its expression in pineal photoreceptors, as the vertebrate eye may have evolved from the pineal-like "eye" of a common ancestor of hagfish and lampreys (Lamb et al.,

2007). The overall conclusion from these ideas is that ARR4 may manifest distinctive features of the most ancient subfamily of the arrestins, and in particular, its role in quenching cone opsin activity.

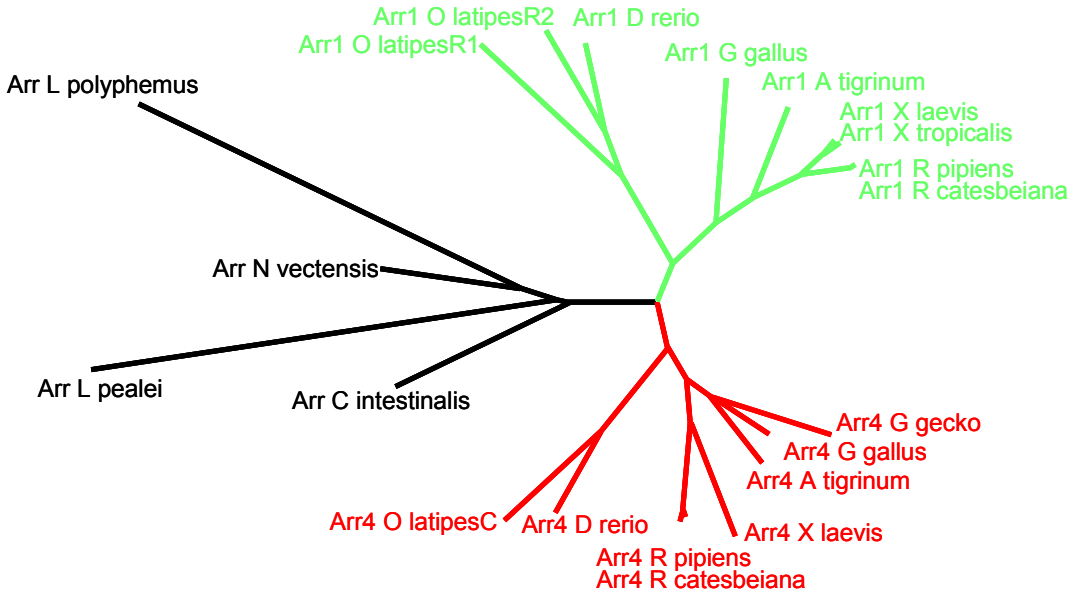

Figure 11S. Phylogenetic analysis of arrestin sequences from lower organisms. Primary sequences of arrestin proteins from the indicated species were aligned and an unrooted phylogenetic tree generated using ClustalW (Thompson et al., 1994). Tree data were rendered with Dendroscope (Huson et al., 2007) . Subtrees are color-coded according to visual arrestin type (Arr1 – green, Arr4 – red) where such designation has been reported; the branches in black correspond to species in which identified visual arrestin sequences have either not been assigned, or species whose ancestors diverged from the line leading to vertebrates prior to the divergence of the Arr1 and Arr4 sequences. R1, R2, and C designations for the *O. latipes* sequences are as described by the authors (Imanishi et al., 1999).

References

Barnes,S. (1994). After transduction: response shaping and control of transmission by ion channels of the photoreceptor inner segments. Neuroscience *58*, 447-459.

Craft,C.M., and Whitmore,D.H. (1995). The arrestin superfamily: cone arrestins are a fourth family. FEBS Lett *362*, 247-255.

Delsuc,F., Brinkmann,H., Chourrout,D., and Philippe,H. (2006). Tunicates and not cephalochordates are the closest living relatives of vertebrates. Nature *439*, 965-968.

Donoso,L.A., Gregerson,D.S., Smith,L., Robertson,S., Knospe,V., Vrabec,T., and Kalsow,C.M. (1990). S-antigen: preparation and characterization of site-specific monoclonal antibodies. Curr. Eye Res *9*, 343-355.

Gasteiger,E., Hoogland,C., Gattiker,A., Duvaud,S., Wilkins,M.R., Appel,R.D., and Bairoch,A. (2005). Protein identification and analysis tools on the ExPASy Server. In The Proteomics Protocols Handbook, J.M. Walker, ed. (Totowa, NJ: Humana Press), pp. 571-607.

Gregerson,D.S., Knospe,V., and Donoso,L.A. (1989). Selection of antibody epitopes in an immunopathogenic neural autoantigen. J. Neuroimmunol. *24*, 191-206.

Guex,N., and Peitsch,M.C. (1996). A fast and easy-to-use PDB Viewer for Macintosh and PC. Protein Data Bank Quarterly Newsletter *77*, 7-15.

Gurevich,E.V., and Gurevich,V.V. (2006). Arrestins: ubiquitous regulators of cellular signaling pathways. Genome Biol. *7*, 236.

Gurevich,V.V., and Benovic,J.L. (2000). Arrestin: mutagenesis, expression, purification and functional characterization. In Methods in Enzymology, K. Palczewski, ed. pp. 422-437.

Gurevich,V.V., Orsini,J.J., and Benovic,J.L. (1999). Characterization of arrestin expression and function. In Receptor Biochemistry and Methodology, pp. 157-178.

Hanson,S.M., Gurevich,E.V., Vishnivetskiy,S.A., Ahmed,M.R., Song,X., and Gurevich,V.V. (2007). Each rhodopsin molecule binds its own arrestin. Proc. Natl. Acad. Sci. U. S A *104*, 3125-3128.

Hirsch,J.A., Schubert,C., Gurevich,V.V., and Sigler,P.B. (1999). The 2.8 A crystal structure of visual arrestin: a model for arrestin's regulation. Cell *97*, 257-269.

Huson,D.H., Richter,D.C., Rausch,C., Dezulian,T., Franz,M., and Rupp,R. (2007). Dendroscope: An interactive viewer for large phylogenetic trees. BMC Bioinformatics *8*, 460.

Imanishi,Y., Hisatomi,O., and Tokunaga,F. (1999). Two types of arrestins expressed in medaka rod photoreceptors. FEBS Lett *462*, 31-36.

Kassai,H., Aiba,A., Nakao,K., Nakamura,K., Katsuki,M., Xiong,W.H., Yau,K.W., Imai,H., Shichida,Y., Satomi,Y., Takao,T., Okano,T., and Fukada,Y. (2005). Farnesylation of retinal transducin underlies its translocation during light adaptation. Neuron *47*, 529-539.

Krispel,C.M., Chen,D., Melling,N., Chen,Y.J., Martemyanov,K.A., Quillinan,N., Arshavsky,V.Y., Wensel,T.G., Chen,C.K., and Burns,M.E. (2006). RGS expression rate-limits recovery of rod photoresponses. Neuron *51*, 409-416.

Lamb,T.D., Collin,S.P., and Pugh,E.N., Jr. (2007). Evolution of the vertebrate eye: opsins, photoreceptors, retina and eye cup. Nat. Rev. Neurosci. *8*, 960-976.

Lyubarsky,A.L., Daniele,L.L., and Pugh,E.N., Jr. (2004). From candelas to photoisomerizations in the mouse eye by rhodopsin bleaching in situ and the light-rearing dependence of the major components of the mouse ERG. Vision Res *44*, 3235-3251.

Nair,K.S., Hanson,S.M., Mendez,A., Gurevich,E.V., Kennedy,M.J., Shestopalov,V.I., Vishnivetskiy,S.A., Chen,J., Hurley,J.B., Gurevich,V.V., and Slepak,V.Z. (2005). Light-dependent redistribution of arrestin in vertebrate rods is an energy-independent process governed by protein-protein interactions. Neuron *46*, 555-567.

Nikonov,S.S., Daniele,L.L., Zhu,X.M., Craft,C.M., Swaroop,A., and Pugh,E.N. (2005). Photoreceptors of Nrl(-/-) mice coexpress functional S- and M-cone opsins having distinct inactivation mechanisms. Journal of General Physiology *125*, 287-304.

Nikonov,S.S., Kholodenko,R., Lem,J., and Pugh,E.N. (2006). Physiological features of the S- and M-cone photoreceptors of wild-type mice from single-cell recordings. Journal of General Physiology *127*, 359-374.

Nir,I., and Ransom,N. (1992). S-antigen in rods and cones of the primate retina: different labeling patterns are revealed with antibodies directed against specific domains in the molecule. Journal of Histochemistry & Cytochemistry. 40(3):343-52.

Pawley,J.B. (2007). Handbook of Biological Confocal Microscopy (New York: Plenum).

Pierce,E.A., Quinn,T., Meehan,T., McGee,T.L., Berson,E.L., and Dryja,T.P. (1999). Mutations in a gene encoding a new oxygen-regulated photoreceptor protein cause dominant retinitis pigmentosa. Nat. Genet. *22*, 248-254.

Reichenbach,A., and Robinson,S.R. (1995). Phylogenetic constraints on retinal organization and development. Progress in Retinal and Eye Research *15*, 139-171.

Sidow,A. (1996). Gen(om)e duplications in the evolution of early vertebrates. Curr. Opin. Genet. Dev. *6*, 715-722.

Strissel,K.J., Sokolov,M., Trieu,L.H., and Arshavsky,V.Y. (2006). Arrestin translocation is induced at a critical threshold of visual signaling and is superstoichiometric to bleached rhodopsin. J. Neurosci. *26*, 1146-1153.

Thompson,J.D., Higgins,D.G., and Gibson,T.J. (1994). CLUSTAL W: improving the sensitivity of progressive multiple sequence alignment through sequence weighting, position-specific gap penalties and weight matrix choice. Nucleic Acids Res *22*, 4673-4680.

Zhu,X., Li,A., Brown,B., Weiss,E.R., Osawa,S., and Craft,C.M. (2002). Mouse cone arrestin expression pattern: light induced translocation in cone photoreceptors. Mol. Vis. *8*, 462-471.